공학석사 학위논문

Effects of Different Chalcogen Atom Substitution in Electron Rich Unit of Isoindigo-based Conjugated Copolymer on Photovoltaic Properties

아이소인디고 기반 공액고분자 내의 16족 원소의 치환에 따른 광전 특성

2014년 2월

서울대학교 대학원

재료공학부

유 태 웅

Abstract

Effects of Different Chalcogen Atom Substitution in Electron Rich Unit of Isoindigo-based Conjugated Copolymer on Photovoltaic Properties

Yoo, Tae Woong

Department of Materials Science and Engineering

Seoul National University

Recently, chalcogen atom substitution on a conjugated copolymer is investigated to enhance the photovoltaic properties. In this study, new low bandgap conjugated copolymers based on isoindigo and chalcogenophenes (thiophene, selenophene and tellurophene) were synthesized (PIT, PISe and PITe, respectively) to investigate the effects of the chalcogen atom on the photovoltaic properties. The copolymers PISe and PITe show both bathochromic shift and lowering the lowest unoccupied molecular orbital energy level as compared to its thiophene analogue. The solar cell device based on PISe blended with $PC_{61}BM$ exhibits enhanced power conversion efficiency (PCE) of 4.36% with a J_{SC} of 9.38 mA cm^{-2} which is higher than that of PIT. However, PITe shows lower J_{SC} than that of PIT and PISe because of its coarse morphology of the blend.

Keywords: chalcogenophene, isoindigo, conjugated copolymer, polymer solar cells

Student Number: 2012-20615

Contents

List of Schemes

List of Figures

List of Tables

1. Introduction

Solution-processed bulk-heterojunction (BHJ) organic photovoltaics (OPVs) are very attractive as a renewable energy source due to the promising advantages such as low cost manufacturing, light weight and flexibility.[1-3] One of the key parts in OPVs is the *p*-type material as an electron donor which absorbs photon.[4] In the 1990s, poly(*p*-phenylenevinylene)s (PPVs) was extensively studied. However, power conversion efficiency (PCE) of PPV-based BHJ OPVs was achieved as high as 3.3% with $PC_{61}BM$ as the electron acceptor material. The high bandgap (2.2 eV) of PPVs limited the short-circuit current density (J_{SC}) to 5–6 mA/cm^2.[5] To reduce bandgap of polymer, polythiophenes (PTs) was investigated. One of the most successful PTs for OPVs is the regioregular poly(3-hexylythiophene) (P3HT). P3HT-based bulk heterojunction (BHJ) OPVs provide a higher current density than PPVs because of its lower bandgap (2.0 eV) and increased crystallinity which yields a higher hole mobility. When the BHJ OPV was fabricated using P3HT, the J_{SC} of device is increased over 10 mA/cm^2. As a result, PCEs of P3HT were reported to 4–5% with optimized morphology of active layer which is achieved after thermal or solvent annealing.[6-7]

Recent progress in performance of OPVs has been achieved by designing of novel low-bandgap conjugated polymers to maximize the light absorption, especially at longer wavelength where much of the photon flux emitted from the sun, and offer high J_{SC}.[8] In the molecular designing point of

view, there are several methods that can achieve the low-bandgap conjugated polymers: (**1**) combination of electron-rich unit (donor) and electron-deficient unit (acceptor),[8] (**2**) rigidification of the polymer backbone to promoting the interchain π-πstacking,[9] (**3**) substitution by electron donating and/or accepting side groups to tuning the HOMO and/or LUMO energy level of polymer.[10] Among these methods, the combination of the donor and acceptor is the easy way to achieve the low bandgap conjugated polymer.

The donor-acceptor (D-A) concept for reduction of the bandgap was proposed by Havinga et al. in 1992.[11] The basic principle of the D-A concept is based on the internal charge transfer (ICT) from donor to acceptor. According to this principle, the HOMO and LUMO energy levels of polymer can be tuned readily by controlling the ICT interaction. The HOMO energy level of the donor will interact with that of the acceptor to generate two new occupied molecular orbitals after covalent bond. One of them is higher and the other is lower than the two initial HOMO energy levels before molecular orbital hybridization. The two LUMO energy levels would be generated in a similar manner. And this effect leads to formation of higher HOMO energy level and lower LUMO energy level in the whole conjugated main chain, and consequently bandgap of polymer narrows.[12] In the D-A concept, the HOMO and LUMO energy level of D-A copolymers is mainly governed by the donor and acceptor, respectively. Therefore, to modify the energy level of polymer, a variety of donor and acceptor units were investigated. Recently, fluorene,[13] carbazole,[14] benzo[1,2-*b*:4,5-*b*']dithiophene (BDT),[15] cyclopenta[2,1-*b*:3,4-*b*']dithiophene (CPDT),[16] dithieno[3,2-*b*:2',3'-*d*]silole

(DTS)[17] were used as donor units, while 2,1,3-benzothiadiazole (BT),[18] thieno[3,4-*c*]pyrrole-4,6-dione (TPD),[19] diketopyrrolo[3,4-c]pyrrole,[20] isoindigo[21] were used as acceptor units for alternating copolymers.

Isoindigo, which contains two strong electron-withdrawing lactam rings with a planar π-conjugated structure, is a useful acceptor unit for D-A type low-bandgap polymers. Reynolds and his co-workers reported that the isoindigo-based oligomer based organic solar cells and showed promising absorption spectra and favorable electrochemical and photovoltaic properties.[22] Later, many isoindigo containing conjugated polymers were synthesized and used for OPVs, and the highest PCE was found to be 7.09%.[23] This result demonstrated the promising potential of the isoindigo unit as an electron-deficient unit for D-A type of polymer toward high efficient OPVs.

Several studies of selenium-containing polymer have exhibited promising properties for use in organic photovoltaics. For example, selenium-containing polymers should have lower bandgap than the sulfur-containing analogues. This reduced bandgap of polymer is accomplished by lowering the LUMO energy level while maintaining the HOMO energy level.[24-25] As a result, absorption of photons in long wavelength region would be increased and provide the increased J_{SC}. In addition, interchain-charge transfer should be facilitated by intermolecular Se-Se interactions, leading to an enhanced hole mobility that is desirable for high photocurrent.[26] While thiophene and selenophene based polymers have emerged in recent years, one of the tellurium-containing heterocyclic compounds, tellurophene, has

been rarely reported.[27-28] The selenium atom is similar to the sulfur atom and therefore many properties of selenophene are similar to those of thiophene. However, the tellurium atom is significantly different from those of sulfur and selenium. For instance, the electronegativities of S and Se are 2.58 and 2.55, respectively, whereas that of Te is 2.10. And tellurium is a metalloid, therefore, tellurium has the capability to form hypervalent coordination complexes, which enable strong interchain interaction.[29] In addition, tellurophene has a lower bandgap than thiophene, thus the optical absorption of tellurophene should be red-shifted compared to that of thiophene. Considering all of these properties of selenium and tellurium, they become promising substituents for sulfur in electron rich unit for high performance OPVs.

In this study, isoindigo-based D-A type conjugated copolymers with heterocyclic compounds containing a series of chalcogen atoms, including sulfur, selenium and tellurium which are thiophene, selenophene and tellurophene, were designed and synthesized. For high J_{SC}, sulfur atom in polymer is substituted to selenium and tellurium which is expected to have a lower LUMO energy level. The optical, electrochemical and charge transport properties of polymers as well as photovoltaic performance of the OPVs are examined. Also the morphological study of the polymer/PCBM blend was performed to understand the performance of the OPV device based on isoindigo-based conjugated polymers. Consequently, the new D-A type copolymers with selenophene and isoindigo showed the best J_{SC}.

2. Experimental Section

2.1. Materials

All reagents were obtained from Sigma-Aldrich, Alfa-Aesar, TCI chemicals, and Acros Organics and used as received. Tetrahydrofuran (THF) (Dejung Chemicals & Metals) was dried over sodium/benzophenone under nitrogen and freshly distilled before use. The reagents of 6-bromo-2-oxindole, 6-bromoisatin, thiophene, selenophene, tellurium, $NaBH_4$ and 1,4-dichloro-2-butyne were used as received. The chemicals used as solvents for the reactions including polymerization were anhydrous and purchased from the Sigma-Aldrich.

2.2. Synthesis of monomers

2.2.1. Synthesis of 1-bromo-2-hexyldecane (1)

2-hexyl-1-decanol (20 g, 82.49 mmol) and triphenylphosphine (43.27 g, 16.50 mmol) were dissolved in dichloromethane (50 ml) and cooled in ice-water bath. To the mixture *N*-bromosuccinimide (22.02 g, 123 mmol) was added slowly, then stirred at room temperature for 24 h. Removal of the solvent afforded the crude product which was further purified using column chromatography on silica gel using a hexane as eluent, giving the product as colorless oil. (24.68 g, 98%) ^{1}H-NMR (300 MHz, $CDCl_3$) δ: 3.45 (br, 2H), 1.57 (d, 1H), 1.27 (m, 24H), 0.88 (m, 6H)

2.2.2. Synthesis of 6,6'-dibromo-1H,1'H-[3,3']biindolylidene-2,2'-dione (2)

Scheme 2.1 shows the synthesis route of 6,6'-dibromo-1,1'-bis(2-hexyldecyl)-[3,3'-biindolinylidene]-2,2'-dione (**3** in scheme 2.1). The compound 2 was synthesized by aldol condensation reaction, as shown in scheme 2.1. To a 250 mL two-neck round-bottomed flask was added 6-bromo-2-oxindole (1 g, 4.72 mmol) and 6-bromoisatin (1.066 g, 4.72 mmol). The flask was evacuated and filled with nitrogen. Acetic acid (30 mL) and conc. HCl solution (0.2 mL) was added. Then, the reaction mixture was stirred and heated under reflux for 24 h. The mixture was cooled to room temperature and filtered. The solid material was washed with water, ethanol and diethyl ether. After residual solvent was dried under reduced pressure, the crude product 2 was obtained. (1.902 g, 95%) ^{1}H-NMR (300 MHz, DMSO-*d*6) δ: 11.08 (br, 2H), 9.01 (d, 2H), 7.20 (d, 2H), 7.00 (s, 2H)

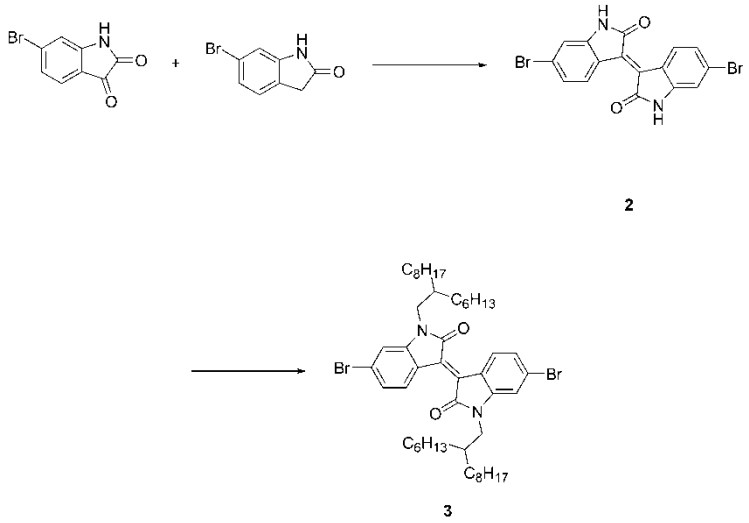

Scheme 2.1 The synthesis route of 6,6'-dibromo-1,1'-bis-(2-hexyl-decyl)-1H,1'H-[3,3']biindolylidene-2,2'-dione

2.2.3. Synthesis of 6,6'-dibromo-1,1'-bis-(2-hexyl-decyl)-1H,1'H-[3,3']biindolylidene-2,2'-dione (3)

To a 250 mL two-neck round-bottomed flask under nitrogen atmosphere was added compound 2 (1 g, 2.38 mmol), potassium carbonate (987 mg, 7.14 mmol) and dimethylformaldehyde (DMF) (100 mL). Reaction mixture was stirred and heated at 120 ^{o}C for 1 h. Compound 1 (1.6 g, 5.24 mmol) was injected through a septum under nitrogen. The mixture was stirred for 15 h at 120 ^{o}C and then poured into water (200 mL). The organic phase was extracted by diethyl ether, washed with brine and dried over $MgSO_4$. After removal of the solvent under reduced pressure, the deep-red solids were purified by silica chromatography, eluting with (CH_2Cl_2:Hexane = 1:1) to give 6,6'-dibromo-N,N'-(2-hexyldecyl)-isoindigo. (1.76 g, 85%) ^{1}H-NMR (300 MHz, $CDCl_3$) δ: 9.07 (d, 2H), 7.16 (dd, 2H), 6.88 (d, 2H), 7.00 (s, 2H), 3.62 (d, 4H), 1.95-1.80 (m, 2H), 1.45-1.20 (m, 48H), 0.95-0.78 (m, 12H) ^{13}C-NMR (500 MHz, $CDCl_3$) δ: 168.1, 146.2, 132.6, 131.0, 126.7, 125.1, 120.4, 111.5, 44.7, 36.1, 31.8, 31.5, 29.9, 29.6, 29.2, 26.4, 22.6, 14.1 MS (FAB) Calculated for $C_{48}H_{72}Br_2N_2O_2$ [M]+: 868.91, found 869.0

2.2.4. Synthesis of tellurophene (4)

The tellurophene was synthesized as shown in Scheme 2.2. Tellurium (10 g, 78.37 mmol) and $NaBH_4$ (13g, 343.64 mmol) were added in a 500 mL three-neck round-bottomed flask (flask A). A 500 mL 2-neck round bottom flask (flask B) was loaded with potassium hydroxide (19 g, 338.62 mmol) in distilled water (100 mL). A dropping funnel loaded with 1,4-dichloro-2-butyne (13 g, 105.71 mmol) dissolved in 1,4-dioxane (15 mL) was placed in flask B. Gas tube was connected from the top of the condenser on flask B to a stainless needle connected to a side neck of flask A (the needle is submerged into the contents of flask A). A dropping funnel was loaded with nitrogen purged methanol (150 mL) and placed on flask A. Two flasks are purged with N_2 and then deionized water (150 mL) was injected in one portion through a septum to flask A and stirring begun. After 10 min, there was a noticeable discharge of hydrogen gas occurring and the water began to boil. After 20 min, the tellurium was completely reduced giving a violet solution. At this point, flask A was cooled in an ice bath and methanol (150 mL) was added. At the same time, flask B was brought to reflux and 1,4-dichloro-2-butyne was slowly added for 10 min. After another 20 min, the ice bath was removed from flask A and the reaction left alone for 2 h as the buta-1,3-diyne was being introduced from flask B. After the 2 h, flask B was removed from the heat and flask A was exposed to air. The resulting black suspension in flask A was filtered over Celite and extracted with hexane after addition of brine. The organic layer was dried over $MgSO_4$ and the solvent was removed by evaporation. The resulting red liquid was purified by

column chromatography to give desired compound 4 as a light red liquid. (4.93 g, 35%) ^{1}H-NMR (300 MHz, $CDCl_3$) δ: 8.97 (dd, 2H), 7.84 (dd, 2H)

2.2.5. Synthesis of 2,5-bis(trimethylstannyl)thiophene (5)

2,5-bis(trimethylstannyl)thiophene (5) was synthesized similarly to a method described in the literature by Seitz at al.[30] To a 100 mL two-neck round-bottomed flask under nitrogen atmosphere was added thiophene (1 g, 11.89 mmol) and tetramethylethylenediamine (TMEDA) (3.74 mL, 24.96 mmol) in dried THF (15 mL) at 0 ^{o}C. *n*-BuLi (10 mL, 25 mmol, 2.5 M in hexanes) was added dropwise to a solution and the reaction mixture was heated to reflux for 45 min. After cool down to 0 ^{o}C, trimethyltin chloride (25 mL, 25 mmol, 1.0 M in THF) was added slowly. After stirring overnight at room temperature, saturated aqueous ammonium chloride (50 mL) was added to the flask. The organic layer was washed with $CuSO_4$ until no more precipitate appeared, dried over $MgSO_4$, filtered over Celite and concentrated to 5 mL on rotary evaporator. The solution was recrystallized from hexanes to afford a white solid. (4.38 g, 90%) ^{1}H-NMR (300 MHz, $CDCl_3$) δ: 7.37 (s, 2H), 0.36 (s, 18H)

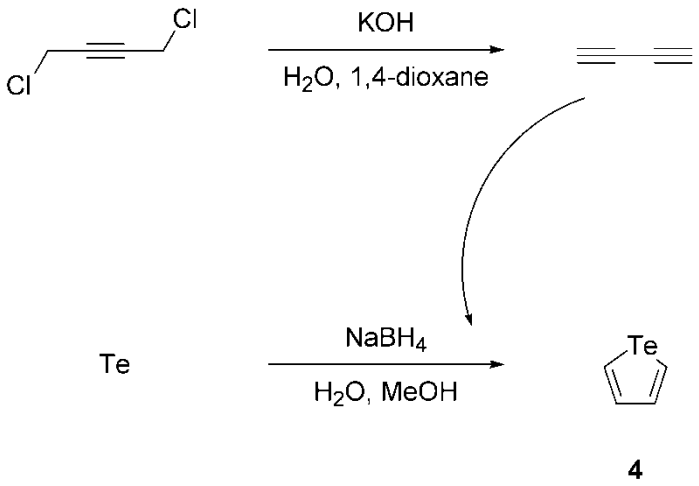

Scheme 2.2 The synthetic scheme of tellurophene

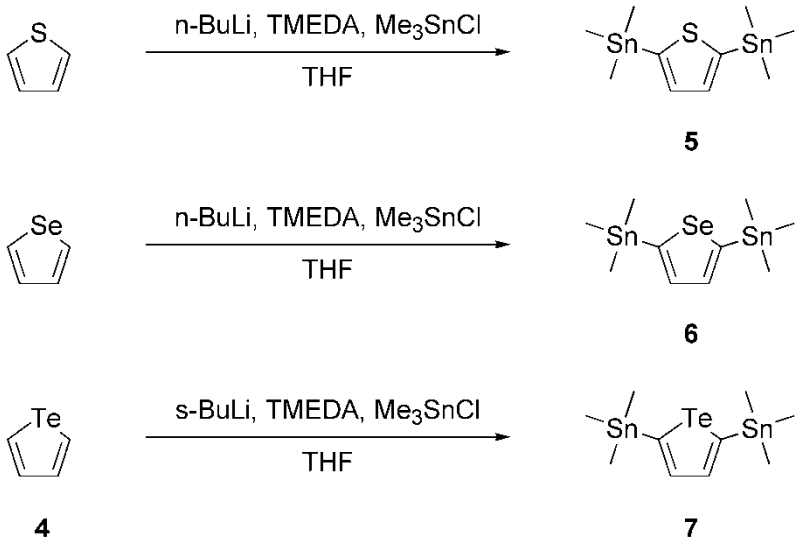

Scheme 2.3 The synthetic scheme of stannylation

2.2.6. Synthesis of 2,5-bis(trimethylstannyl)selenophene (6)

To a 100 mL two-neck round-bottomed flask under nitrogen atmosphere was added selenophene (1 g, 7.63 mmol) and tetramethylethylenediamine (TMEDA) (2.4 mL, 16.02 mmol) in dried THF (15 mL) at 0 ^{o}C. *n*-BuLi (6.4 mL, 16 mmol, 2.5 M in hexanes) was added dropwise to a solution and the reaction mixture was heated to reflux for 45 min. After cool down to 0 ^{o}C, trimethyltin chloride (16 mL, 16 mmol, 1.0 M in THF) was added slowly. After stirring overnight at room temperature, saturated aqueous ammonium chloride (50 mL) was added to the flask. The organic layer was washed with aqueous solution of $CuSO_4$ until no more precipitate appeared, dried over $MgSO_4$, filtered over Celite and concentrated to 5 mL on rotary evaporator. The solution was recrystallized from hexanes to afford a white solid. (2.79 g, 80%) ^{1}H-NMR (300 MHz, $CDCl_3$) δ: 7.67 (s, 2H), 0.36 (s, 18H)

2.2.7. Synthesis of 2,5-bis(trimethylstannyl)tellurophene (7)

To a 100 mL three-neck round-bottom flask was added compound 4 (1 g, 5.57 mmol), TMEDA (1.75 mL, 11.70 mmol) and 30 mL dried THF. Under nitrogen, the mixture was chilled in an ice–water bath and *s*-BuLi (8.4 mL, 11.75mmol, 1.4 M in cyclohexane) was added dropwise by dropping funnel. The resulting light colored suspension was then heated to near reflux for 45 min. The dark-brown mixture was then chilled in an ice-bath again and trimethyltin chloride (11.75 mL, 11.75 mmol, 1 M in hexanes) was slowly added by dropping funnel. After stirring overnight at room temperature, saturated aqueous ammonium chloride (50 mL) was added to the flask. The layers were separated and the organic layer was washed with aqueous solution of $CuSO_4$ until no more precipitate appeared. The extract was filtered over Celite, washed with water, dried over Na_2SO_4 and concentrated to 5 mL on a rotary evaporator. The solution was recrystallized from methanol to afford a white solid. (1.41 g, 50%) ^{1}H NMR (300 MHz, CDCl3): d = 8.31 (s, 2 H), 0.34 (s, 18 H).

2.3. Synthesis of polymers

Isoindigo-based semiconducting polymers, poly(1,1'-Bis-(2-hexyl-decyl)-6-thiophen-2-yl-1H,1'H-[3,3']biindolylidene-2,2'-dione) (PIT), poly(1,1'-Bis-(2-hexyl-decyl)-6-selenophene-2-yl-1H,1'H-[3,3']biindolylidene-2,2'-dione) (PISe) and poly(1,1'-Bis-(2-hexyl-decyl)-6-tellurophene-2-yl-1H,1'H-[3,3']biindolylidene-2,2'-dione) (PITe), were synthesized via the Stille coupling between dibrominated isoindigo (3) and distannylated aromatic hetero cyclic compound (5, 6 and 7).

2.3.1. Synthesis of PIT

The compound 3 (150 mg, 0.173 mmol), the compound 5 (70.7 mg, 0.173 mmol) and tri(*o*-tolyl)phosphine (10 mg) in anhydrous toluene (4 mL) were charged in microwave reactor vial. The mixture was purged for 10 min and tris(dibenzylideneacetone)dipalladium(0) ($Pd_2(dba)_3$) (6 mg) was added. The mixture was heated at 140 ^oC for 12 h in microwave reactor. After cooled down to room temperature, three drops of 2-trimethylstannylthiophene was added and the mixture was heated at 140 ^oC for 30 min in microwave reactor. After the reaction complete, five drops of 2-bromothiophene was added in microwave reactor vial and the mixture was heated at 140 ^oC for 30 min. The resulting mixture was poured into methanol (250 mL) and the precipitate was collected in a Soxhlet thimble filter. And then the precipitate was extracted with methanol, acetone and hexane until the extracts were colorless. After that, the polymer was extracted with chloroform. The chloroform fraction was reduced in volume and precipitated

in methanol and filtered over a 4.5μm PTFE filter and dried under vacuum at 50 ^{o}C overnight. (120 mg, 87.4%)

2.3.2. Synthesis of PISe

The compound 3 (150 mg, 0.173 mmol), the compound 6 (79 mg, 0.173 mmol) and tri(o-tolyl)phosphine (10 mg) in anhydrous toluene (4 mL) were charged in microwave reactor vial. The mixture was purged for 10 min and tris(dibenzylideneacetone)dipalladium(0) ($Pd_2(dba)_3$) (6 mg) was added. The mixture was heated at 140 ^{o}C for 12 h in microwave reactor. After cooled down to room temperature, three drops of 2-trimethylstannylthiophene was added and the mixture was heated at 140 ^{o}C for 30 min in microwave reactor. After the reaction complete, five drops of 2-bromothiophene was added in microwave reactor vial and the mixture was heated at 140 ^{o}C for 30 min. The resulting mixture was poured into methanol (250 mL) and the precipitate was collected in a Soxhlet thimble filter. And then the precipitate was extracted with methanol, acetone and hexane until the extracts were colorless. After that, the polymer was extracted with chloroform. The chloroform fraction was reduced in volume and precipitated in methanol and filtered over a 4.5μm PTFE filter and dried under vacuum at 50 ^{o}C overnight. (115 mg, 79.1%)

2.3.3. Synthesis of PITe

The compound 3 (150 mg, 0.173 mmol), the compound 7 (87.4 mg, 0.173 mmol) and in anhydrous toluene (4 mL) were charged in microwave reactor vial. The mixture was purged for 10 min and tetrakis(triphenylphosphine)palladium(0) ($Pd(PPh_3)_4$) (10 mg) was added. The mixture was heated at 140 ^oC for 12 h in microwave reactor. After cooled down to room temperature, three drops of 2-trimethylstannylthiophene was added and the mixture was heated at 140 ^oC for 30 min in microwave reactor. After the reaction complete, five drops of 2-bromothiophene was added in microwave reactor vial and the mixture was heated at 140 ^oC for 30 min. The resulting mixture was poured into methanol (250 mL) and the precipitate was collected in a Soxhlet thimble filter. And then the precipitate was extracted with methanol, acetone and hexane until the extracts were colorless. After that, the polymer was extracted with chloroform. The chloroform fraction was reduced in volume and precipitated in methanol and filtered over a 4.5μm PTFE filter and dried under vacuum at 50 ^oC overnight. (132 mg, 85.8%)

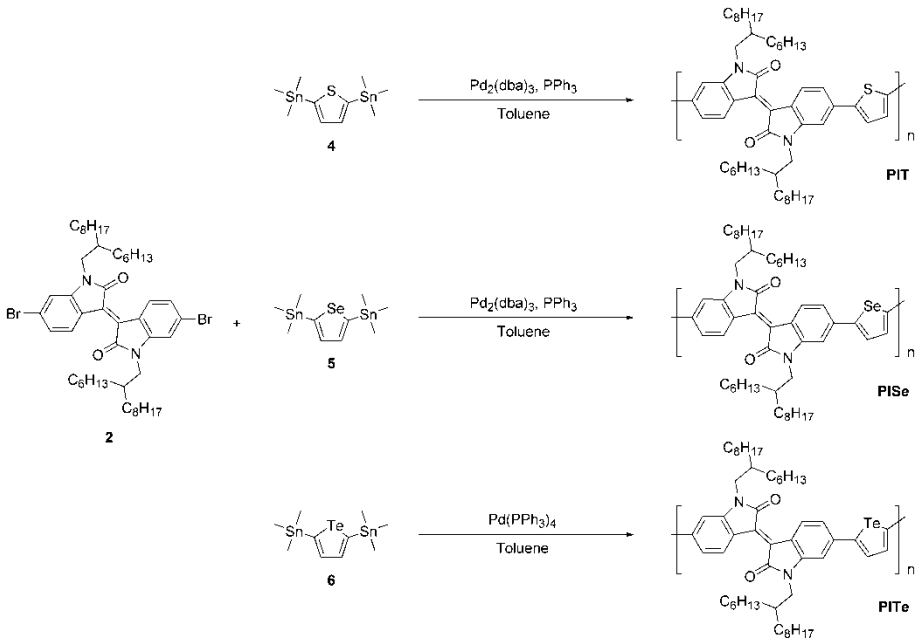

Scheme 2.4 The synthetic scheme of polymers

2.4. Characterization

The chemical structures of the monomers were identified by ^{1}H NMR (Avance DPX-300) and ^{13}C NMR (Avance DPX-500). Mass analysis was performed on JEOL, JMS-600W mass analyzer. Molecular weight and its distribution were measured by gel permeation chromatography (GPC) (Waters) equipped with a Waters 2414 refractive index detector using $CHCl_3$ as an eluent, where the columns were calibrated against standard polystyrene samples. The optical absorption spectra were obtained by UV-Vis spectrophotometer (Lambda 25, Perkin Elmer). Cyclic voltammetry experiments were carried out on potentiostat/galvanostat (VMP 3 Biologic) in an electrolyte solution of 0.1 M tetrabutylammonium hexafluorophosphate (Bu_4NPF_6) in acetonitrile. A three-electrode setup was used with platinum wires (Bioanalytical System Inc.) both as working and counter electrode. And Ag/Ag^{+} was used as reference electrode calibrated with ferrocene/ferrocenyl couple (Fc/Fc^{+}). X-ray diffraction (XRD) patterns were obtained from an X-ray diffractometer (New D8 Advance, Bruker) using Cu-Kα radiation (λ= 1.5418 Å) at a scan rate of 2° min^{-1}. Thin film morphology was characterized by transmission electron microscopy (TEM) with a JEOL JEM1010 operating in 80 kV of acceleration voltage. For TEM measurement, the solar cell device was immersed in deionized water and then the active layer was floated onto the Cu grid.

2.5. Device fabrication and measurements

2.5.1. Materials

ITO-patterned glass was used as an anode in OPV device. The sheet resistance of the ITO was less than 10 Ω sq^{-1}. [6,6]-phenyl-C_{61}-butyric acid methyl ester ($PC_{61}BM$) (>99.5%) was obtained from Nano-C and used as received. PEDOT:PSS (Clevios P VP AI 4083) was purchased from H.C. Stark and passed through a 0.45 μm PVDF syringe filter before spin-coating.

2.5.2. Solar cell device fabrication

Photovoltaic devices were fabricated on ITO coated glass substrate with a layered structure of ITO/PEDOT:PSS/polymer:$PC_{61}BM$/Ca/Al. The ITO coated glass substrate was cleaned by stepwise sonication in acetone and IPA for 15 min each. After complete drying, the ITO coated glass substrate was treated with UV-ozone for 15 min. PEDOT:PSS was spin-coated onto the ITO with 40 nm in thickness, and the substrate was annealed at 150 ^{o}C for 10 min in a N_2-filled glove box. Polymers and $PC_{61}BM$ were dissolved in anhydrous *o*-dichlorobenzene (*o*-DCB) and the solution was stirred at 70 ^{o}C for 4 h. Then solution was spin-coated on the top of the PEDOT:PSS layer. Ca (20 nm in thickness) was thermally evaporated under vacuum lower than 10^{-6} Torr on the top of the active layer, then Al (100 nm) was thermally deposited on the Ca layer. The active area of cell was ca. 4 mm^2.

2.5.3. Solar cell performance measurements

The photovoltaic performance was measured under nitrogen atmosphere inside the glove box. The current density–voltage (*J–V*) curves of the device were obtained on a computer-controlled Keithley 4200 source measurement unit under AM 1.5G (100 mW cm^{-2}) simulated by an Oriel solar simulator (Oriel 91160A). The light intensity was calibrated using a NREL-certified photodiode prior to each measurement. The external quantum efficiency (EQE) was measured using Polaronix K3100 IPCE measurement system (McScience). The light intensity at each wavelength was calibrated with a standard single-crystal Si cell.

2.5.4. Field effect transistor (FET) device fabrication and characterization

Bottom-gate/top-contact organic FET was fabricated using heavily doped Si wafer as the bottom gate electrode with 250 nm of SiO_2 layer as the gate dielectric. The substrate was cleaned in piranha solution (H_2SO_4:H_2O_2 = 1:1) and acetone for 20 min and dried in oven 120 ^oC for 1 h. The wafer was treated with UV-ozone for 20 min, and then the wafer was immersed in 0.1 mM octadecyltrichlorosilane (OTS) solution in anhydrous toluene. Thin films of the polymer were deposited on the OTS treated substrates by spin-coating using a polymer solution (5 mg mL^{-1}) in $CHCl_3$, followed by thermal annealing at 150 ^oC under nitrogen atmosphere. After polymer thin film deposition, the 40 nm thick gold top contact was thermally evaporated in vacuum through a shadow mask. OFETs were characterized under nitrogen atmosphere using Keitheley 4200 and MST5000A.

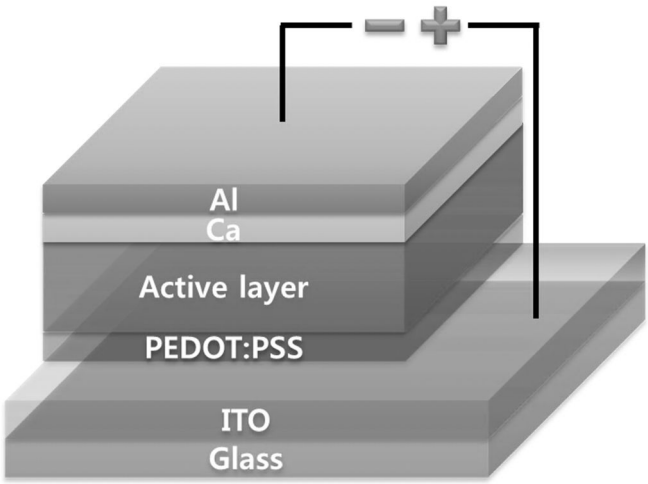

Fig 2.1 Schematic illustration of structure of OPV device

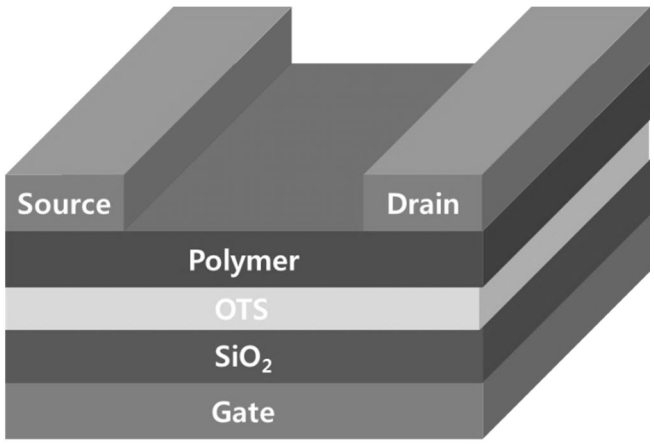

Fig 2.2 Schematic illustration of structure of OFET device

3. Results and Discussion

3.1. Synthesis and Characterization

The compound 2 was prepared by aldol condensation reaction of 6-bromo-2-oxindole and 6-bromoisatin at 120 ^{o}C. Since compound 2 has poor solubility in common organic solvent, the isoindigo should have the solubilizing groups such as alkyl chains. Therefore, we prepared the 1-bromo-2-hexyldecane (1), which is converted from the 2-hexyldecanol. The compound 3, isoindigo with long alkyl chains, was prepared under the mild basic condition using DMF as a solvent. The compound 5,6 and 7 which have distannyl group for Stille coupling were prepared by lithiation through the addition of butyl lithium followed by reaction with trimethylthin chloride at 0 ^{o}C. After the recrystallization of the crude product from hexane, the compound 5, 6 and 7 were obtained in needle-like crystal.

The chemical structure of 1-bromo-2-hexyldecane (1), 6,6'-dibromo-1H,1'H-[3,3']biindolylidene-2,2'-dione (2), 6,6'-dibromo-1,1'-bis-(2-hexyl-decyl)-1H,1'H-[3,3']biindolylidene-2,2'-dione (3), tellurophene (4), 2,5-bis(trimethylstannyl)thiophene (5), 2,5-bis(trimethylstannyl)-selenophene (6) and 2,5-bis(trimethylstannyl)tellurophene (7) are identified by ^{1}H-NMR, as shown in Figure 3.1-7, respectively.

The PIT, PISe and PITe were synthesized from isoindigo as an acceptor unit and thiophene, selenophene and tellurophene as a donor unit via microwave-assisted Stille coupling polycondensation. After Soxhlet

extraction which removed the metal catalysts and low molecular weight polymers, high molecular weight polymers were obtained. The number-average molecular weight (M_n) and polydispersity index (PDI) of polymers are determined by GPC as shown in Table 3.1.

3.2. Optoelectical properties

The optical characteristics of the PIT, PISe and PITe were investigated using UV-Vis absorption spectroscopy in $CHCl_3$ solution and film. Theses optoelectrical properties were summarized in Table 3.1. The UV-Vis absorption spectra of the polymers in $CHCl_3$ solution are shown in Figure 3.8 (a). In $CHCl_3$ solution, absorption maximum (λ_{max}) of PIT is 695 nm and absorption onset (λ_{onset}) is 755 nm. In contrast, PISe and PITe exhibit λ_{max} at 705 and 720 nm and λ_{onset} at 780 and 800 nm, respectively. The λ_{max} of PISe and PITe are slightly red-shifted relative to thiophene analogue PIT. In addition, λ_{onset} of PISe and PITe show a bathochromic shift (ca. 25-45 nm) compared to that of PIT. These bathochromic shifts of λ_{max} and λ_{onset} means polymer can absorb more photons in long wavelength region. When the λ_{max} and λ_{onset} of polymers in solution are compared to that in film, it reveals that the spectra of PISe and PITe are slightly red-shifted in solid state while PIT shows similar spectrum. These results show that substitution of sulfur to selenium and tellurium is effective way to shift of the absorption toward longer wavelength. Absorption coefficient is also important as much as absorption spectrum. As shown in Figure 3.8 (a), the absorption coefficient of the PISe (~76 L g^{-1} cm^{-1}) is larger than the PIT (~67 L g^{-1} cm^{-1}) while

absorption coefficient of PITe slightly decreased compared with PIT. The larger absorption coefficient of PISe than that of PIT contributes to the higher J_{SC} in OPVs while absorption coefficient of PITe slightly decreased compared with PIT. Optical bandgaps of PIT, PISe and PITe calculated from λ_{onset} in film are 1.62, 1.58 and 1.53 eV, respectively.

The HOMO energy levels of PIT, PISe and PITe were measured using cyclic voltammetry. The HOMO energy level of the polymer was calculated using the equation:

$$\text{HOMO} = -[E_{ox} - E_{1/2}(\text{ferrocene}) + 4.8] \text{ eV}.$$

As shown in Figure 3.9, the PISe and the PITe have the same HOMO energy level of –5.60 eV which is identical value to that of PIT. The LUMO energy levels calculated from the optical bandgap of the PIT, PISe and PITe are –3.98, –4.02 and –4.07 eV, respectively.

Since the bandgap of polymer is slightly decreased by substitution of sulfur to selenium and tellurium, the absorption of PISe and PITe in long wavelength region is increased than that of PIT. However, the similar HOMO energy level prevents a significant change in the V_{OC} which is related to the difference between the HOMO energy level of the polymer and the LUMO energy level of the $PC_{61}BM$.

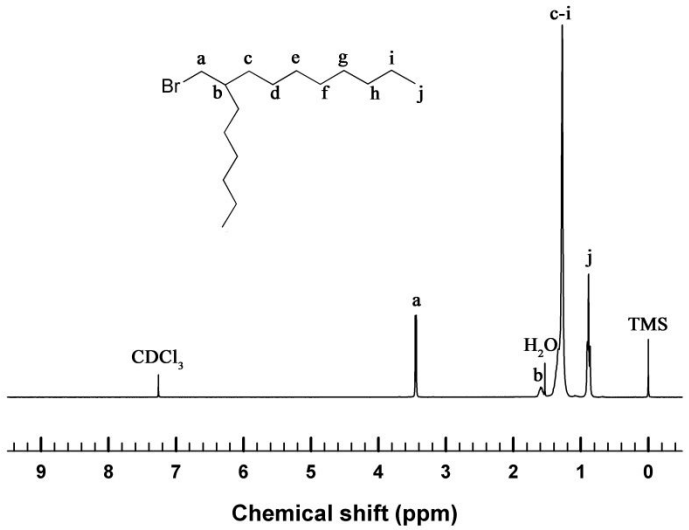

Fig 3.1 Chemical structure and ^{1}H NMR spectrum of compound 1

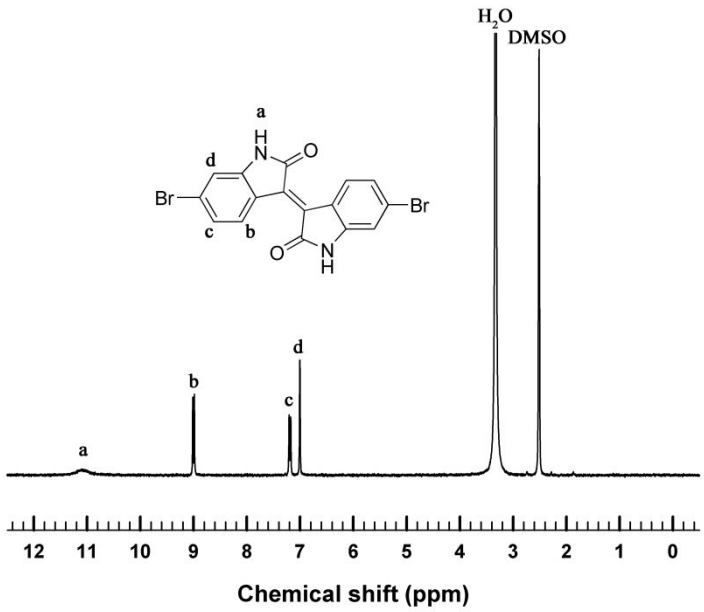

Fig 3.2 Chemical structure and ^{1}H NMR spectrum of compound 2

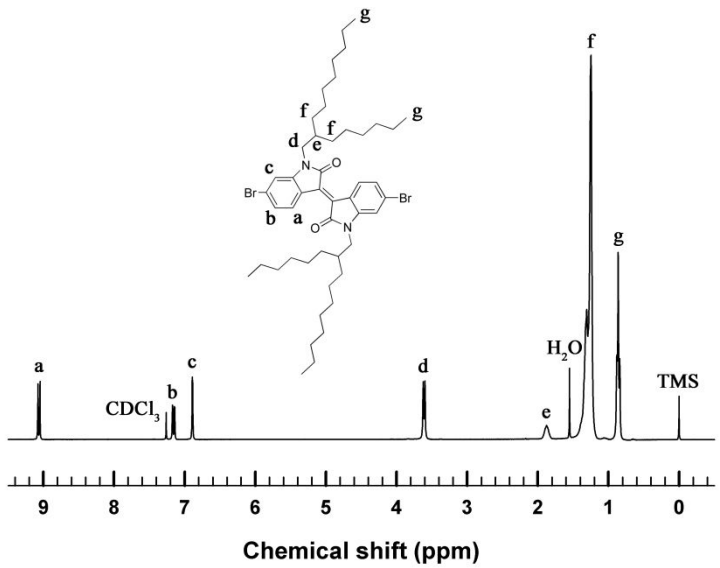

Fig 3.3 Chemical structure and ^{1}H NMR spectrum of compound 3

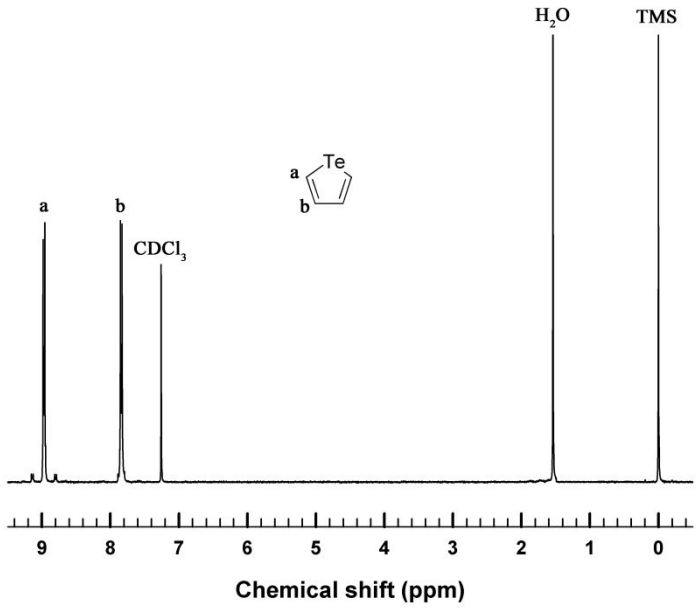

Fig 3.4 Chemical structure and ^{1}H NMR spectrum of compound 4

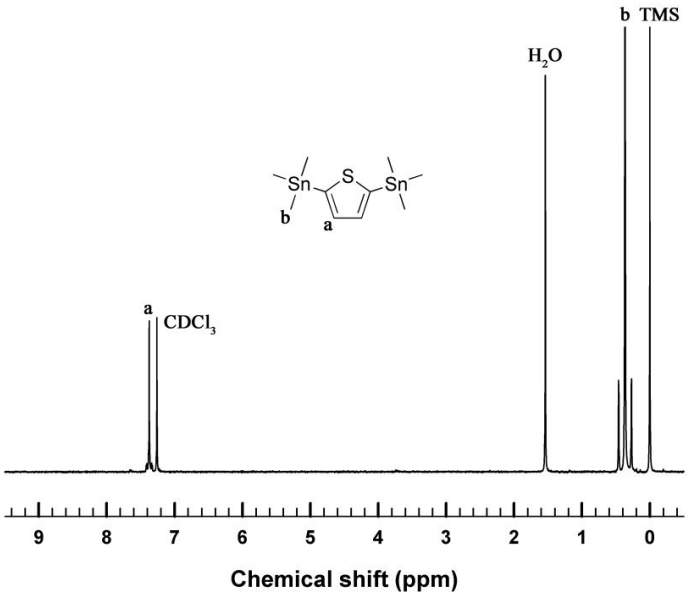

Fig 3.5 Chemical structure and ^{1}H NMR spectrum of compound 5

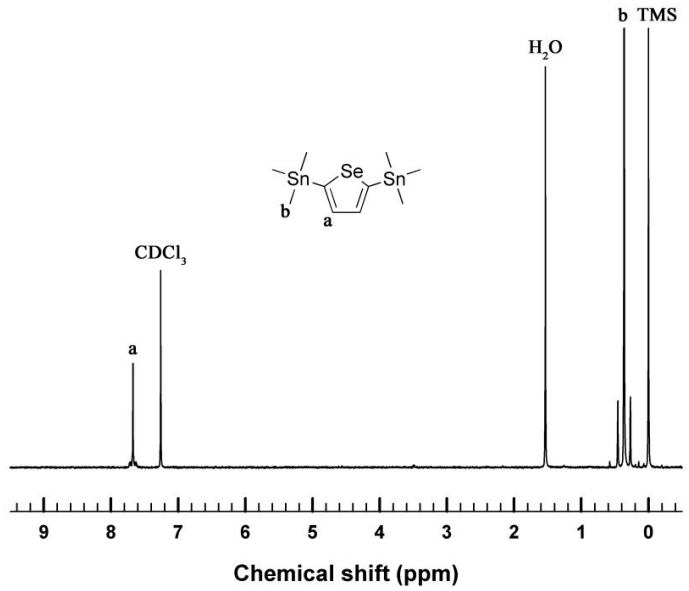

Fig 3.6 Chemical structure and ^{1}H NMR spectrum of compound 6

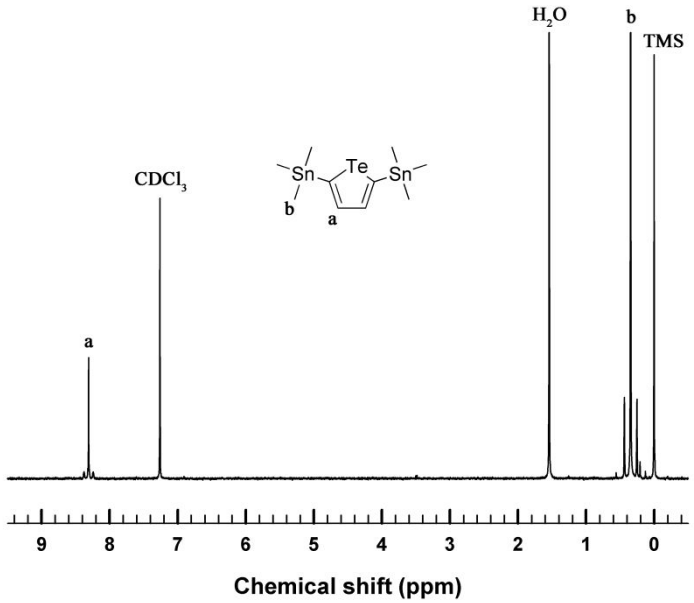

Fig 3.7 Chemical structure and ^{1}H NMR spectrum of compound 7

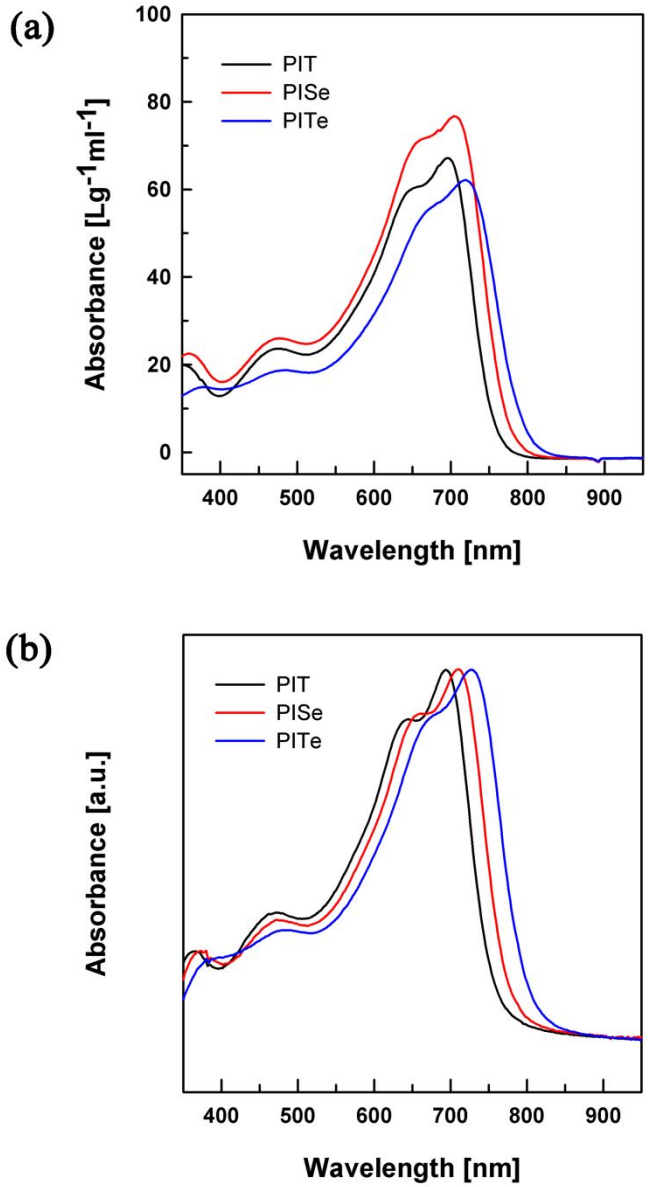

Fig 3.8 UV-Vis absorption spectra of the polymers in (a) $CHCl_3$ solution and (b) film

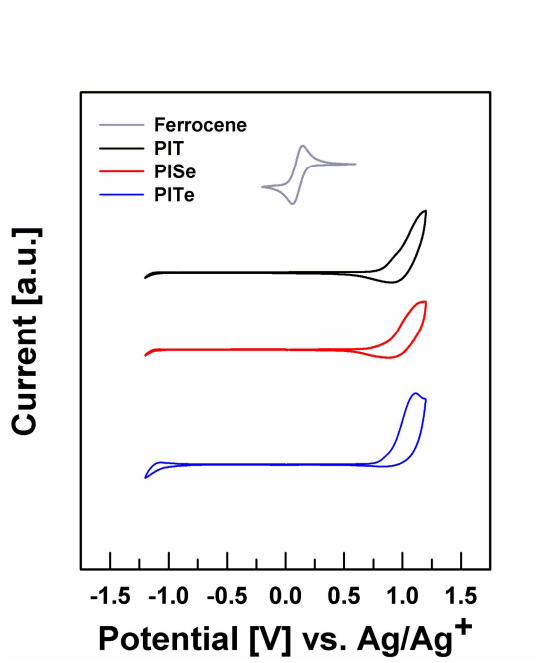

Fig 3.9 Cyclicvoltammograms of PIT, PISe and PITe

Table 3.1 Optical and electrochemical properties of the polymers

Polymer	M_n (kg mol^{-1})	PDI	λ_{max} (nm)		E_g^{opt}	HOMO	LUMO[a]
			solution	film	(eV)	(eV)	(eV)
PIT	86	1.55	755	765	1.62	–5.60	–3.98
PISe	108	1.51	780	785	1.58	–5.60	–4.02
PITe	47	1.60	800	810	1.53	–5.60	–4.07

[a] Calculated from the optical bandgap and the HOMO energy level. LUMO = HOMO + E_g^{opt}

3.3. Structural properties

The crystallinity of the polymer directly affects to the hole mobility as well as the morphology development of the active layer. Therefore, the crystallinity of polymers was investigated using the XRD. Figure 3.10 shows the XRD spectra of thin films of the three polymers which are thermally annealed at 150 ^{o}C for 30 min. The (100) diffraction peak can be seen in all polymers. PIT and PISe films show relatively low crystallinity with maximum reflections up to first order, accompanied by low intensities. This diffraction peak can be assigned as the interchain distance between polymer chains, where alkyl groups are expected to self-organize with an interdigitating manner. When the sulfur atom was substituted to selenium and tellurium, the intensity of (100) diffraction peak related to crystallinity of polymer is increased, and interchain distance of polymer which is calculated from (100) diffraction peak is decreased. Additional (200) and (300) diffraction peak appeared in the PITe thin film. This indicates that the crystallinity of polymer is increased as the sulfur atom is substituted to selenium and tellurium, as a result, mobility related to crystallinity of polymer is expected to increase.

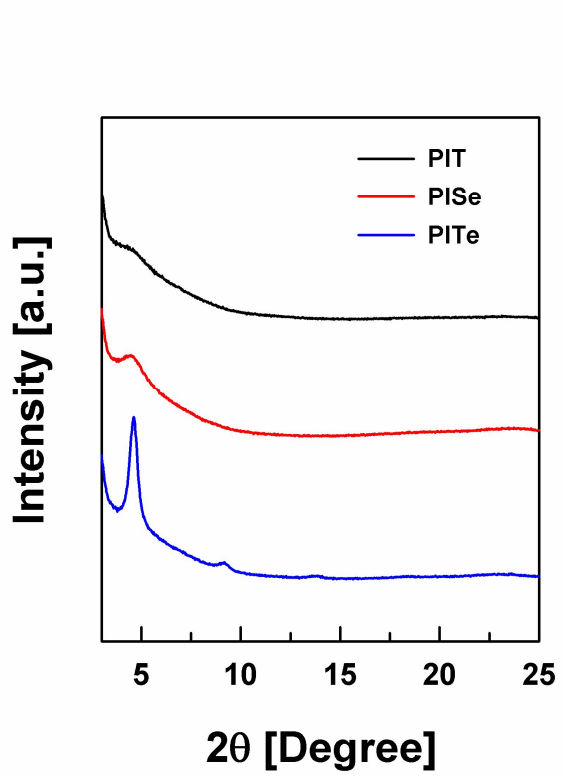

Fig 3.10 X-ray diffraction patterns of PIT, PISe and PITe films

3.4. Photovoltaic properties

The effect of chalcogen atom substitution on the photovoltaic properties was investigated using device configuration of ITO/PEDOT:PSS/ Polymer:$PC_{61}BM$/Ca/Al (Figure 2.1). The devices prepared from polymer:$PC_{61}BM$ using *o*-DCB as a processing solvent. In the optimization of the photovoltaic performance of OPVs, the blend ratio of the polymer to the PCBM is very important. In this study, the optimum ratios of the polymers to $PC_{61}BM$ were found to be 1 to 1 for PIT and PISe, while 1 to 4 for PITe. The *J*–*V* curves of these devices are shown in Figure 3.11 and photovoltaic parameters are summarized in Table 3.2. The V_{OC}s of devices are quite similar because of the same HOMO energy levels (–5.60 eV) of polymers. The solar cell device of PISe with $PC_{61}BM$ exhibited a PCE of 4.36% with J_{SC} of 9.38 mA cm^{-2} and FF of 50%, which is the highest PCE among the devices. The increase of PCE is mainly result from J_{SC} which is increased about 12% as compared to the PIT. This higher J_{SC} of PISe is attributed to more absorption of photon at longer wavelength region as compared to PIT. Meanwhile, despite of the increased absorption at longer wavelength compared to PIT, the PITe showed 1.16% of PCE with J_{SC} of 2.51 mA cm^{-2}. The corresponding EQE spectra are shown in Figure 3.12 for each solar cell devices. The EQE spectra indicate that the OPV device of PISe has showed broad response from 300 to 800 nm while the PIT showed light response less than 760 nm.

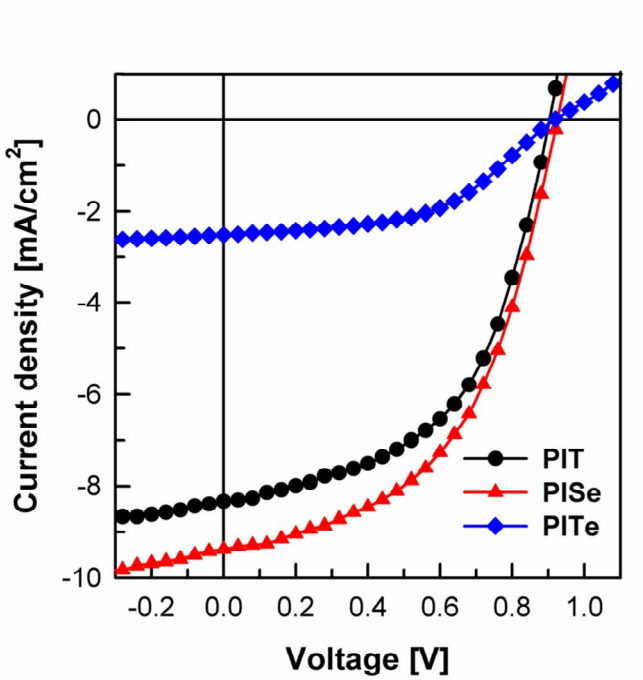

Fig 3.11 *J–V* curves measured under AM 1.5 G (100 mW cm^{-2}) of OPV devices based on PIT, PISe and PITe

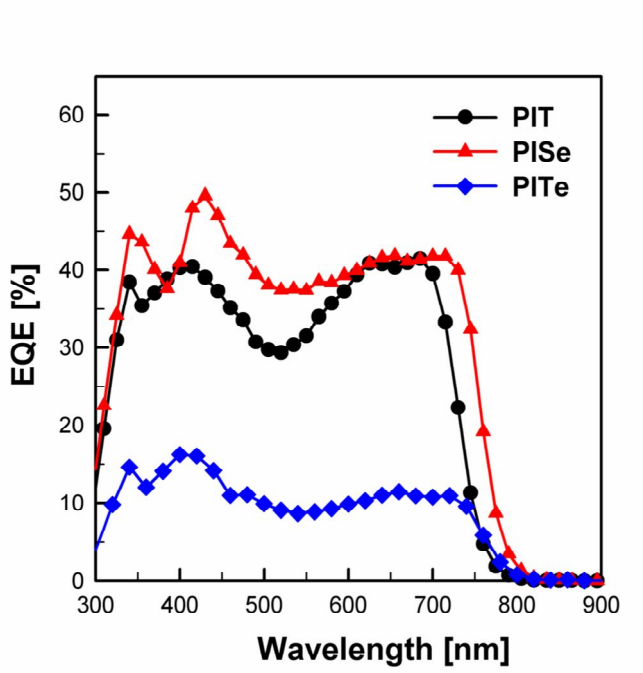

Fig 3.12 EQE spectra of OPV devices with PIT, PISe and PITe

Table 3.2 Summary of photovoltaic properties of PIT, PISe and PITe blended with $PC_{61}BM$

Polymer	Blend ratio (polymer:$PC_{61}BM$)	V_{OC} (V)	J_{SC} (mA cm^{-2})	FF (%)	PCE (%)
PIT	1:1	0.90	8.34	53	3.98
PISe	1:1	0.93	9.38	50	4.36
PITe	1:4	0.92	2.51	50	1.16

3.5. Charge transport characteristics

The performance of OPVs is related to the charge carrier mobility. To investigate the vertical direction charge carrier transport characteristics of the polymer thin films, the hole mobility was measured by the standard method from single charge carrier device. The device configuration of hole only device was ITO/PEDOT:PSS/polymer:$PC_{61}BM$/Au. The hole mobility was measured from the space charge limited current (SCLC) *J–V* curve which was obtained in the dark. The SCLC behavior is analyzed using the Mott-Gurney law,[33-34]

$$J = (9/8)\varepsilon_0\varepsilon_r\mu_h(V^2/L^3)$$

where ε_0 is vacuum permittivity, ε_r is dielectric constant of the polymer (assumed 3 for PIT, PISe and PITe), μ_h is drift mobility of charge carrier, $V = V_a - V_{bi}$ (V_a: applied bias, V_{bi}: built-in potential), and L is the thickness of the film. The hole mobilities of the PIT, PISe and PITe calculated from *J–V* curve (Figure 3.14 (a)) are 1.22×10^{-6}, 2.35×10^{-6} and 2.89×10^{-7} $cm^2 V^{-1} s^{-1}$, respectively. The higher hole mobility of the PISe than PIT is because the PISe has the higher crystallinity than that of the PIT, and this higher mobility may also contribute to higher J_{SC} of PISe than that of PIT. Despite of the good crystallinity, the PITe exhibited poor hole mobility because of the coarse morphology of blend film.

To verify the charge carrier mobility through the direction parallel to the substrate, FET devices with the configuration of bottom-gate and top-contact device were fabricated on heavily n-doped conductive silicon wafer with 250

nm SiO_2. The thin films of PIT, PISe and PITe were deposited onto OTS modified silicon substrates by spin-coating dilute polymers solution (5 mg mL^{-1} in chloroform) yielding ~30 nm thickness. The devices were annealed at 150 ^oC to increase the intermolecular packing, which resulted in higher mobility.[35] The charge carrier mobilities were evaluated from the transfer curves of source–drain current vs. gate voltage (I_{SD} vs. V_G) in well-resolved saturation regime according to the equation,

$$I_{SD} = (W/2L)C_i\mu(V_G - V_T)^2$$

where I_{SD} is the drain current in the saturated regime, W and L are the semiconductor channel width and length, C_i is the capacitance (C_i = 10.8 nF cm^{-2}) of the gate dielectric layer, and V_G and V_T are the gate voltage and threshold voltage. As shown in Figure 3.15 (a), pristine film of polymers did not exhibit observable field effect behavior. Previous study of PIT showed similar result.[36] However, after annealing at 150 ^oC, the FET devices made of PIT, PISe and PITe exhibited a typical p-channel transistor behavior with moderate hole carrier mobility (see Figure 3.15 (b)). As discussed above, the reason for this change is the post-annealing of the thin film causes intermolecular packing and enhances the field effect mobility in the OFET device. The hole mobilities of annealed PIT, PISe and PITe films were 0.003, 0.016 and 0.072 $cm^2 V^{-1} s^{-1}$, respectively. The mobilities of PISe and PITe are higher than that of PIT. This is because the PISe and PITe have relatively higher crystallinity than PIT. The OFET mobility of PIT in this study is lower than that of previously studied PIT (0.015 $cm^2 V^{-1} s^{-1}$). Despite PITe

shows higher mobility than that of PIT and PISe, PITe exhibits lower J_{SC}. Therefore, another factor might influence on the low J_{SC} of PIT.

In OFET device, the self-assembled monolayer (SAM) is modifying the SiO_2 dielectric surface and such modifications usually result in increased charge carrier mobility for a variety of solution-cast organic semiconductors. This SAM has been shown to reduce dielectric surface traps such as interfacial trapped H_2O, and to tune surface energy and control surface roughness.[37-38] Consequently, the mobility difference in same polymer may arise from the fabrication conditions such as the surface treatment and surface quality. In order to improve the OFET mobility, further optimization in device fabrication is required.

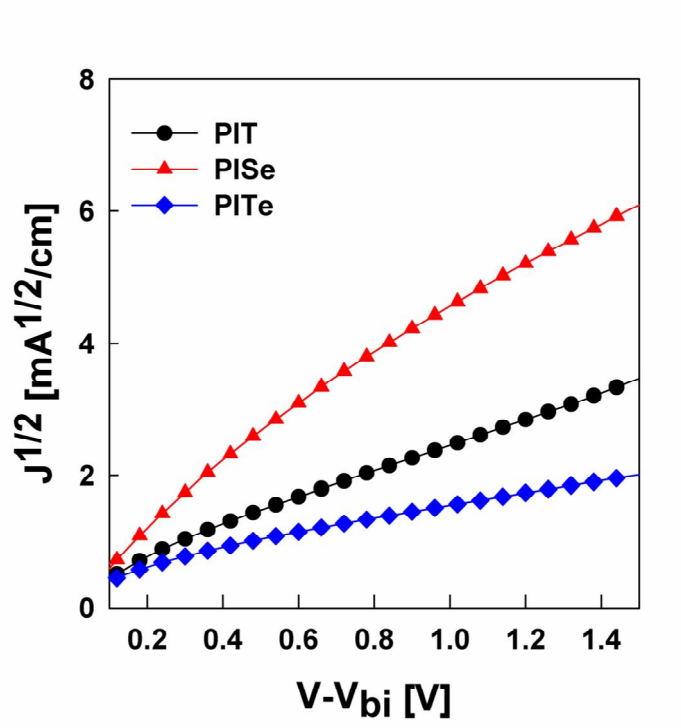

Fig 3.13 Dark current density–voltage curves from SCLC devices of polymer:$PC_{61}BM$ blend film

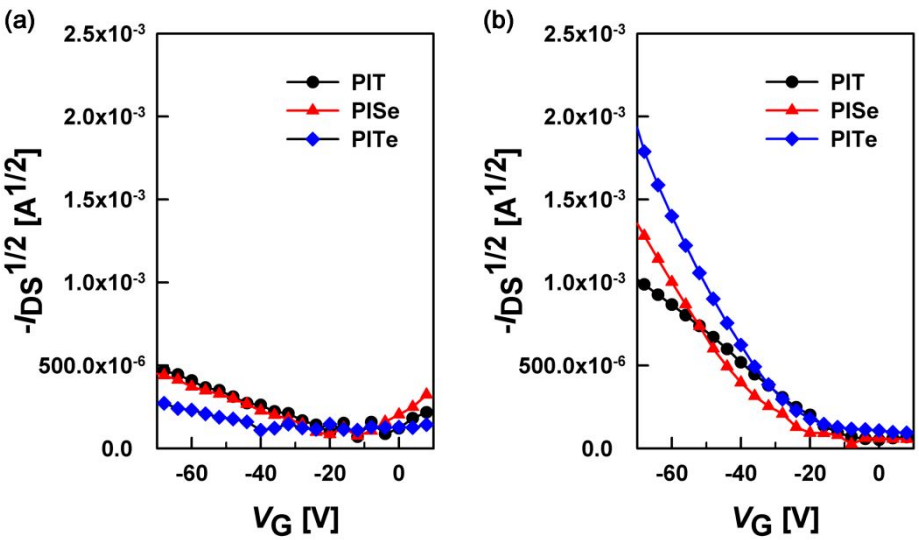

Fig 3.14 Transfer curves from FET devices of (a) pristine and (b) 150 ^{o}C annealed polymer thin films

3.6. Morphology investigation

The thin film morphology of the conjugated polymer is an important factor for the performance of the OPV device. To investigate the morphology of the blend film, we used TEM. As shown in Figure 3.12, the bright regions can be attributed to the polymer domains, while the dark regions can be attributed to the $PC_{61}BM$ domains due to its high electron scattering density.[31] The PIT film blended with $PC_{61}BM$ cast from *o*-DCB without the DIO additive exhibited a coarse morphology, as shown in Figure 3.13 (a), indicating the formation of large separate domains of aggregated polymer and $PC_{61}BM$. To improve the morphology of film, a small amount of diiodooctane (DIO) was added into the solution. It has been reported that the morphology of active layer can be modified and optimized by the use of additive.[32] When the casting solvent is DCB with a small amount (2.5 vol.%) of DIO additive, the PIT showed uniform and fine feature which is indicating nanoscale phase separation and resulted in an effective interaction between the PIT and $PC_{61}BM$ (Figure 3.132 (b)). It is because that the mixed solvent of *o*-DCB and DIO promotes self-assembly of the polymers. Similarly, nanoscale interconnected network structure between the PISe and $PC_{61}BM$ was well developed (Figure 3.13 (c)). While the PITe showed relatively large scale phase separation (Figure 3.13 (d)). The well-developed interconnected network structure affords not only high J_{SC} but also high FF. Therefore, the PIT and PISe showed higher J_{SC} than PITe.

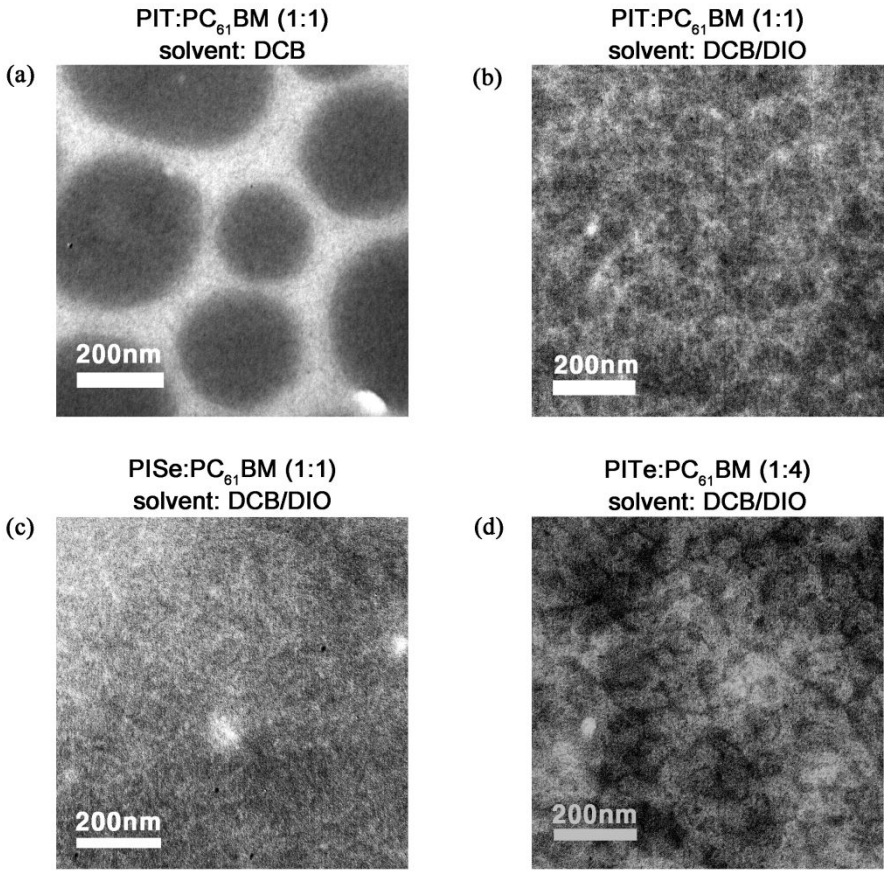

Fig 3.15 TEM images of polymers blended with $PC_{61}BM$ with different weight ratio and different solvent mixtures

4. Conclusions

In this study, a series of low bandgap conjugated copolymers composed of isoindigo and aromatic heterocyclic compound with different chalcogen atom were synthesized. A correlation between the chalcogen atoms and the optoelectrical, crystallinity and photovoltaic performance was found. As the sulfur substituted to selenium and tellurium, the LUMO energy level of the conjugated copolymers becomes lower, crystallinity is increased and thereby photovoltaic properties are changed. The polymer with selenium substitution, PISe, exhibits 4.36% of PCE with increased J_{SC} compared with PIT. However, the PITe based OPV showed the lowest PCE of 1.16%, mainly owing to its small J_{SC} which may arise from poor morphology of blend film, i.e., large phase separation. The PITe thin film exhibits the highest p-type charge transporting behavior with a hole mobility of 0.072 $cm^2\ V^{-1}\ s^{-1}$. Relatively high mobility of PITe based OFET device can be attributed to the higher crystallinity of PITe than that of PIT. Consequently, substitution of chalcogen atoms in conjugated copolymer can be another important approach to control the LUMO energy level, crystallinity and photovoltaic properties.

Bibliography

(1) Yu, G.; Gao, J.; Hummelen. H. C.; Wudl. F.; Heeger. A. J. *Science* **1995**, 270, 1789

(2) Mayukh. M.; Jung. I. H.; He. F.; Yu. L. *J. Polym. Sci. Part B polym. Phys.* **2012**, 50, 1057.

(3) Shaheen, S. E. ; Ginley, D. S. ; Jabbour, G. E. *MRS Bull*. **2005**, 30, 10

(4) Hoppe, H.; Sariciftci, N. S. *J. Mater. Chem.* **2006**, 16, 45.

(5) Brabec, C. J.; Shaheen, S. E.; Winder, C.; Sariciftci, N. S. *Appl. Phys. Lett.* **2002**, 80, 1288.

(6) Ma, W.; Yang, C.; Gong, X.; Lee, K.; Heeger, A. J. *Adv. Funct. Mater.* **2005**, 15, 1617.

(7) Campoy-quiles, M.; Ferenczi, T.; Agostinelli, T.; Etchegoin, P. G.; Kim, Y.; Anthopoulos, T. D.; Stavrinou, P. N.; Bradley, D. D. C.; Nelson, J. *Nat. Mater.* **2008**, 7, 158.

(8) Beaujuge, P. M.; Fréchet, J. M. J. *J. Am. Chem. Soc.* **2011**, 133, 20009.

(9) Chen, Y.; Chang, C.; Cheng, Y.; Hsu, C. *Chem. Mater.* **2012**, 24, 3964.

(10) Liang, Y.; Feng, D.; We, Y.; Tsai, S.; Li, G.; Ray, C.; Yu, L. *J. Am. Chem. Soc.* **2009**, 131, 7792.

(11) Havinga, E. E.; Hoeve, W. T.; Wynberg, H. Polym. Bull.1992, 29, 119

(12) Brocks, G.; Tol, A. *J. Phys. Chem.* **1996**, 100, 1838.

(13) Svensson, M.; Zhang, F.; Veenstra, S. C.; Verhees, W. J. H.; Hummelen, J. C.; Kroon, J. M.; Inganäs, O.; Andersson, M. R. *Adv. Mater.* **2003**, 15, 988.

(14) Blouin, N.; Michaud, A.; Gendron, D.; Wakim, S.; Blair, E.; Neagu-Plesu, R.; Belletête, M.; Durocher, G.; Tao, Y.; Leclerc, M. *J. Am. Chem. Soc.* **2008**, 130, 732.

(15) Zhang, Y.; Hau, S. K.; Yip, H.; Sun, Y.; Acton, O.; Jen, A. K. Y. *Chem. Mater.* **2010**, 22, 2696.

(16) Moulé, A. J.; Tsami, A.; Bunnagel, T. W.; Forster, M.; Kronenberg, N. M.; Scharber, M.; Koppe, M.; Morana, M.; Brabec, C. J.; Meerholz , K.; Scherf, U. *Chem. Mater*, **2008**, 20, 4045.

(17) Chu, T.; Lu, J.; Beaupré, S.; Zhang, Y.; Pouliot, J.; Wakim, S.; Zhou, J.; Leclerc, M.; Li, Z.; Ding, J.; Tao, Y. *J. Am. Chem. Soc.* **2011**, 133, 4250.

(18) Hou, J.; Chen, H.; Zhang, S.; Li, G.; Yang, Y. *J. Am. Chem. Soc.* **2008**, 130, 16144.

(19) Zhang, Y.; Zou, J.; Yip, H.; Sun, Y.; Davies, J. A.; Chen, K.; Acton, O.; Jen, A. K. -Y. *J. Mater. Chem.* **2011**, 21, 3895.

(20) Jung, J. W.; Jo, J. W.; Liu, F.; Russell. T. P.; Jo, W. H. *Chem.*

Commun. **2012**, 48, 6933.

(21) Ma, Z.; Wang, E.; Vandewal, K.; Andersson, M. R.; Zhang, F. *Appl. Phys. Lett.* **2011**, 99, 143302.

(22) Mei, J.; Graham, K. R.; Stalder, R.; Reynolds, J. R. *Org. Lett.* **2010**, 12, 661.

(23) Jung, E. H.; Jo, W. H. *Energy Environ. Sci.* **2013**, DOI: 10.1039/C3EE42297F.

(24) Heeney, M.; Zhang, W.; Crouch, D. J.; Chabinye, M. L.; Gordeyev, S.; Hamilton, R.; Higgins, S. J.; McCulloch, I.; Skabara. P. J.; Sparrowe, D.; Tierney, S. *Chem. Commun.* **2007**, 43, 5061.

(25) Intemann, J. J.; Yao, K.; Yip, H. L.; Xu, Y. X.; Li, Y. X.; Liang, P. W.; Ding, F. Z.; Li, X.; Jen, A. K. -Y. *Chem. Mater.* **2013**, 25, 3188.

(26) Patra, A.; Bendikov, M. *J. Mater. Chem.* **2010**, 20, 422.

(27) Hahnke, A. A.; Howe, G. W.; Seferos, D. S. *Angew. Chem. Int. Ed.* **2010**, 49, 10140.

(28) Jahnke, A. A.; Djukic, B.; McCormick, T. M.; Domingo, E. B.; Hellmann, C.; Lee, Y.; Seferos, D. S. *J. Am. Chem. Soc.* **2013**, 135, 951.

(29) Srivastava, P. C.; Bajpai, S.; Bajpai, S.; Ram, C.; Kumar, R.; Jasinski, J. P.; Butcher, R. J. *J. Organomet. Chem.* **2004**, 689, 194.

(30) Seitz, D. E.; Lee, S. H.; Hanson, R. N.; Bottaro, J. C.; *Synth. Commun.* **1983**, 13, 121.

(31) Yang, X.; Loos, J.; Veenstra, S. C.; Verhees, W. J. H.; Wienk, M. M.; Kroon, J. M.; Michels, M. A. J.; Janssen, R. A. J. *Nano Lett*, **2005**, 5, 579.

(32) Lee, J. K.; Ma, W. L.; Brabec, C. J.; Yuen, J.; Moon, J. S.; Kim, J. Y.; Lee, K.; Bazan, G. C.; Heeger, A. J. *J. Am. Chem. Soc.* **2008**, 130, 3619.

(33) Shrotriya, V.; Wu, E. H. E.; Li, G.; Yao, Y.; Yang, Y. *Appl. Phys. Lett.* **2006**, 88, 064104.

(34) Kymakis, E.; Servati, P.; Tzanetakis, P.; Koudoumas, E.; Kornilios, N.; Rompogiannakis, I.; Franghiadakis, Y.; Amaraunga, G. A. J. *Nanotechnology*, **2007**, 18, 435702.

(35) Kang, S. J.; Noh, M.; Park, D. S.; Kim, H. J.; Whang, C. N. *J. Appl. Phys.* **2004**, 95, 2993

(36) Lei, T.; Cao, Y.; Fan, Y.; Liu, C. J.; Yuan, S. C.; Pei, J. *J. Am. Chem. Soc.* **2011**, 133, 6099.

(37) Tang, M. L.; Okamoto, T.; Bao, Z. *J. Am. Chem. Soc.* **2006**, 128, 16002.

(38) Ong, B. S.; Wu, Y. L.; Liu, P.; Gardner, S. *J. Am. Chem. Soc.* **2004**, 126, 3378.

초 록

본 논문에서는 유기태양전지의 광활성층에 사용하는 전도성 고분자의 주쇄에 16족 원소인 sulfur, selenium 그리고 tellurium을 각각 치환함으로써 원소의 주기에 따른 전기적, 광전지적 변화에 대하여 알아보았다. 이를 위해 isoindigo와 thiophene, selenophene 그리고 tellurophene을 각각 palladium 촉매를 이용한 Stille coupling을 통하여 공중합하였다. 고분자의 특성을 알아보기 위하여 GPC, UV-Vis spectroscopy, Cyclic voltammetry, XRD를 이용하여 분석하였다. 광학적 특성의 분석 결과 치환된 원소의 주기가 증가함에 따라서 흡수 파장 시작점이 760 nm에서 810 nm로 이동하였다. 전기화학적 특성은 원소의 주기와 관계 없이 –5.60 eV의 동일한 HOMO energy level을 가지는 반면 주기가 증가함에 따라서 LUMO energy level이 감소하는 것을 확인하였다. 또한 XRD 분석을 통해 원소의 주기의 증가가 고분자의 결정성을 증가시키는 것을 확인하였다.

각각의 고분자와 $PC_{61}BM$을 이용하여 벌크 이종접합의 광활성층을 가지는 유기태양전지 소자를 제작하여 그 특성을 측정한 결과 PISe에서 가장 높은 효율인 4.63%를 나타내었다. 또한 유기박막트렌지스터 소자를 이용하여 정공 이동도를 측정한 결과 PITe가 가장 높은 정공 이동도 ($0.072\ cm^2\ V^{-1}\ s^{-1}$)를 보였다.

주요어: chalcogenophene, isoindigo, 전도성 고분자, 유기태양전지

학번: 2012-20615